Bandwidth reconfigurable metamaterial arrays

Nathanael J. Smith
The Ohio State University

Dimitris Papantonis
The Ohio State University

John L. Volakis
The Ohio State University

Research Article

Bandwidth Reconfigurable Metamaterial Arrays

Nathanael J. Smith, Dimitris Papantonis, and John L. Volakis

ElectroScience Laboratory, Department of Electrical and Computer Engineering, The Ohio State University,
1330 Kinnear Road, Columbus, OH 43210, USA

Correspondence should be addressed to Nathanael J. Smith; smith.5377@osu.edu

Metamaterial structures provide innovative ways to manipulate electromagnetic wave responses to realize new applications. This paper presents a conformal wideband metamaterial array that achieves as much as 10 : 1 continuous bandwidth. This was done by using interelement coupling to concurrently achieve significant wave slow-down and cancel the inductance stemming from the ground plane. The corresponding equivalent circuit of the resulting array is the same as that of classic metamaterial structures. In this paper, we present a wideband Marchand-type balun with validation measurements demonstrating the metamaterial (MTM) array's bandwidth from 280 MHz to 2800 MHz. Bandwidth reconfiguration of this class of array is then demonstrated achieving a variety of band-pass or band-rejection responses within its original bandwidth. In contrast with previous bandwidth and frequency response reconfigurations, our approach does not change the aperture's or ground plane's geometry, nor does it introduce external filtering structures. Instead, the new responses are realized by making simple circuit changes into the balanced feed integrated with the wideband MTM array. A variety of circuit changes can be employed using MEMS switches or variable lumped loads within the feed and 5 example band-pass and band-rejection responses are presented. These demonstrate the potential of the MTM array's reconfiguration to address a variety of responses.

1. Introduction

Engineered materials, also referred to as metamaterials (MTMs) [1], have been of strong interest to the electromagnetics and optics communities. The last decade has provided a large body of papers on realizing metamaterials to exploit their novel phenomena for all sorts of applications from antennas to radio frequency (RF) filters, frequency selective surfaces, novel optical devices, and terahertz. The special October 2011 IEEE Proceedings issue [1–6] provides a large cross section of the theory and applications of metamaterials as well as their use in achieving miniaturization, wave slow-down, ultrathin ground planes, bandwidth control, cloaking, and other special phenomena using optical nanocircuits and other MTM techniques.

Typically, metamaterial and other miniaturization techniques [7] result in narrow bandwidths. This is also true when more traditional techniques such as meandering/shaping and lumped loading [8–10] are used. Miniaturizations based on metamaterials using combinations of periodic arrangements of dielectrics, magnetic materials, conductors, or lumped circuit elements also suffer from narrow bandwidth [11–18]. Bandwidth reconfiguration is addressed using tunable leaky wave antennas in [19–23]. However, these approaches employ varactors or external field biasing with ferrite substrates resulting in narrow instantaneous bandwidths.

A popular approach to achieve bandwidth or frequency reconfiguration is that of using switches to alter the geometry/current flow of the antenna itself [24, 25]. This approach relies on many different technologies including RF-MEMS [26–32], pin diodes [33, 34], varactors [35–37], and optical switches [38, 39]. The use of frequency selective surfaces for reconfiguration and/or enhancing antenna bandwidth has also been pursued [40]. Recently, microfluidic liquid metals and plasma have been used to reconfigure MTMs for tunable sensors and resonators [41–44] implying a strong potential for their application to antennas.

While there is a large body of reconfigurable antennas (including MTM antennas), their instantaneous bandwidth continues to be small. Specifically, during the past decade

most efforts on reconfiguration focused on extending the antenna bandwidth or in shifting the aperture's frequency response using switches or piezoelectric materials. By contrast, herewith we propose a reconfiguration approach that begins with a wideband metamaterial aperture [45, 46]. Because of this, the bandwidth, defined by (1) (where ω_{max} and ω_{min} are the max and min frequency of operation resp.)

$$B = \frac{(\omega_{max} - \omega_{min})}{\sqrt{\omega_{max}\omega_{min}}}, \tag{1}$$

for each reconfiguration is limited only by that of the original aperture. An essential aspect of this aperture [46] is its conformal nature, simplicity (planar array of dipoles or bowtie elements), relatively small thickness, and wideband Marchand balun. It is referred to as the tightly coupled dipole array (TCDA) [47–49] and when integrated with a wideband balun, we will note it as the TCDA-IB array [49–51].

It is important to note that the TCDA array and its feed variations, even though conformal in nature, have been shown to deliver instantaneous bandwidth that is comparable and even greater than the nonconformal Vivaldi arrays [52, 53]. A version of the Vivaldi arrays such as the BAVA [54] does have much improved performance and achieved an impressive 10 : 1 bandwidth with a $\lambda_{hi}/2$ thick profile at broadside. However, this decade bandwidth comes at the expense of matching as the array is scanned (VSWR = 2.75 at broadside, and VSWR < 4 at $\theta = 45°$ scan). Another recent BAVA design [52] delivers 1.8–8 GHz at broadside (1.875–7.5 GHz at 45° scan) with 4.44 : 1 and 4 : 1 bandwidths, respectively, when VSWR < 2.

When considering conformal and/or planar wideband arrays, a major challenge is the suppression of the common mode that may appear in the feed structure of these arrays. This requires a balanced feed that retains its performance across the entire bandwidth. Various feeding arrangements were employed in [47, 48, 55, 56] to suppress the mode and ensure a balanced feed. However, in all these cases, retaining a low VSWR implied narrower bandwidths that ranged from 2 : 1 up to at most 5 : 1. That is, the actual delivered bandwidth of wideband arrays depends on several parameters: isolated array bandwidth, thickness, feed impedance, common mode suppression, maximum acceptable VSWR, losses, and achievable beam scanning range (θ_{max}). With this in mind, Doane et al. [57, 58] used the following metric to compare wideband arrays:

$$P_A = \frac{B \log(1/|\Gamma_{max}|)}{\cos(\theta_{max})}, \quad \text{lossless arrays}, \tag{2}$$

$$P_A = \frac{B \log(1 - \eta_{min})}{2 \cos(\theta_{max})}, \quad \text{lossy arrays}. \tag{3}$$

In this expression, B is the bandwidth noted above, Γ_{max} refers to the max reflection coefficient at the feed within the aperture band, η_{min} is the efficiency which accounts for various losses and includes the term $(1 - |\Gamma_{max}|^2)$, and "log" implies the natural logarithm. As such, the array's performance is penalized for larger VSWRs or higher losses.
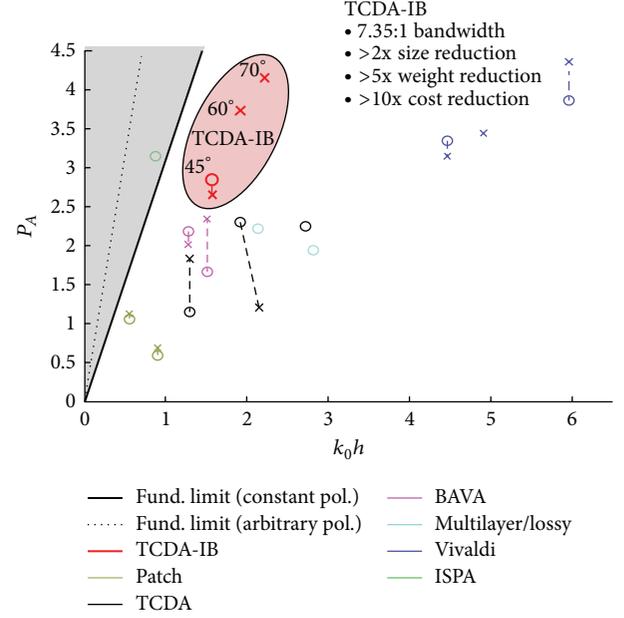

FIGURE 1: Performance factors of selected dual-pol. arrays, alongside fundamental limit from [56]. Here, P_A is a factor proportional to the antenna's bandwidth, B, with penalizations due to mismatches when measured or computed at the scan angle θ_{max}. Γ_{max} refers to the maximum reflection coefficient at the feed across the bandwidth. Note that the symbol "O" refers to broadside performance and symbol "X" refers to the bandwidth performance at the scanning angle of the array as indicated in the figure (see [58] for details). Qualitatively, when the plot symbol is closer to the theoretical optimal line, the antenna's performance is also closer to having optimal performance.

We note that the optimal values for P_A at broadside are [57, 58]

$$P_A \leq \pi\mu_0 k_0 h, \quad \text{constant polarization},$$
$$P_A \leq 2\pi\mu_0 k_0 h, \quad \text{arbitrary polarization}. \tag{4}$$

Figure 1 plots P_A as a function of thickness, h, for various wideband arrays, including the MTM TCDA-IB array. It is seen that variations of the TCDA-IB have larger P_A values for the same thickness (the multilayer/lossy array in Figure 2 refers to the arrays in [49, 59] as they include losses in the substrate). Specifically, the TCDA-IB delivers 6.3 : 1 at broadside, 7.2 : 1 at 30°, and 6.1 : 1 at 60° with VSWRs 2.25, 2.9, and 3.9, respectively. For these TCDA arrays, the superstrate makes them just about $\lambda_{hi}/2$ thick, where λ_{hi} refers to the wavelength at the highest operational frequency. However, if reflections from the ground plane are partially absorbed, much larger bandwidths can be achieved. As an example, the TCDA arrays in [49–51] achieved 21 : 1 bandwidth with 70% efficiency. Indeed, this is a small loss in gain of only 1.5 dB, but the bandwidth is nearly tripled as compared to the lossless case. The ISPA consists of interweaved spirals producing several different polarizations across its UWB and thus is measured against (3) metric for P_A.
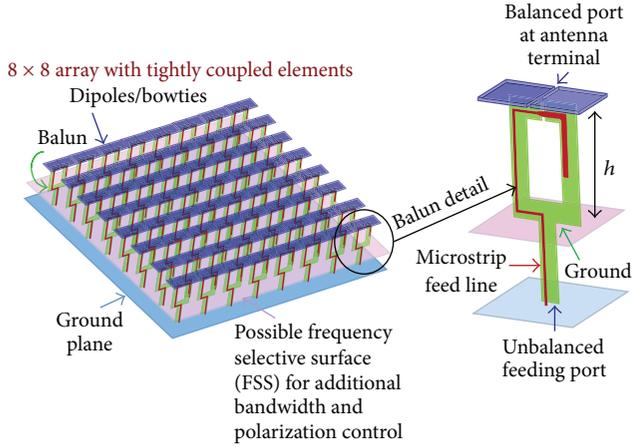
FIGURE 2: Geometrical configuration of the tightly coupled array discussed in [48, 49].

Given that recent MTM arrays can achieve large bandwidth, these apertures can serve as common front-end hardware to accommodate a variety of back-end receivers operating from VHF up to several GHz. Concurrently, there is strong interest to control the array bandwidth for software radio applications, specifically, ensuring that the aperture only operates within the band of interest. As such, it is advantageous to reconfigure its operation or even reduce its large bandwidth, if not needed, to minimize background noise into the receiver. In this paper, we provide a technique for reducing the bandwidth of wideband arrays by reconfiguring its balanced feed placed between the array and ground plane. This is done using switches and LC loads to control the operation of the Marchand [60, 61] balun as displayed Figure 2. It is important to note that our approach departs from traditional methods that shift the bandwidth by integrating switches on the aperture. In the latter case, the switches change the aperture geometry or reconnect the aperture elements to shift the operational bandwidth. Instead, our approach only reconfigures the balun behind the array with a goal to limit its bandwidth or possibly forbid reception over a section of the aperture's original bandwidth.

Below, we begin with a presentation of the MTMs operational concept (Section 2). This is followed by the integrated balun-aperture design of the tightly coupled dipole array (TCDA-IB) and measured performance (Section 3). The reconfiguration concepts and performance are presented in Section 4.

2. Wideband Metamaterial Arrays

Wideband low profile UWB arrays are of interest for many communication and radar functions. As already noted, a challenge in designing UWB arrays is that of maintaining low profiles (small thickness) without reducing bandwidth. It is well known that the bandwidth of low profile apertures can be increased by using magnetic loading [62] to change the phase of the ground plane's reflection coefficient and therefore

introduce constructive addition of the fields directly radiated from the array with those generated by the ground plane. Alternatively, loss within the substrate [63] can be introduced to suppress ground plane reflections. Electromagnetic band gap (EBG) ground planes [64, 65] can also be introduced to reduce array thickness, typically at the expense of bandwidth.

In contrast to modifying or suppressing ground plane reflections, Munk et al. [66] (see also [67]) proposed cancelation of the ground plane's inductance by introducing strong capacitance between the dipoles. This concept is depicted in Figure 3, showing an array of closely placed dipoles, capacitively coupled to each other. The equivalent circuit of the unit cell for this array configuration is represented in Figure 3(b) and consists of shunt inductance (L_2) and capacitance (C_2) along with a series capacitance (C_1) and inductance (L_1). A resistor (R) is included to account for the array's radiation resistance. We note that the shunt inductance (L_2) representing the effect of the ground plane and the series capacitance (C_1) representing the interdipole coupling are the most critical components of the circuit. To achieve large bandwidths, it is necessary for the capacitance C_1 to cancel the effect of the inductance L_2 across a large bandwidth. Specifically, C_1 must vary as a function of frequency to cancel the ground plane inductance of the ground plane $Z_{1+} = j2R_{A0}\tan(2\pi h/\lambda)$, where R_{A0} refers to the characteristic impedance of the medium below the ground plane. That is, referring to Figure 3(c), Z_{1+} must be approximately equal to the conjugate of jX_A. As such, the input impedance seen by the array ports remains nearly real across the bandwidth. We remark that the equivalent circuit shown in Figure 3 is the same as that of metamaterial structures and is the reason for referring to these arrays as MTM structures.

Munk [45, 64] chose to realize the capacitive coupling between the dipoles by placing them close to each other or by interweaving the adjacent dipoles. This is depicted in Figure 4 showing that a VSWR bandwidth of 3 : 1 is achieved. More recently, Munk's array was improved in bandwidth by as much as 10 : 1 bandwidth or more using overlapping dipoles as depicted in Figure 5. This array and feed configuration is discussed in [49, 50].

Summarizing, the TCDA array achieves wide bandwidth by employing the following features.

(i) Interelement Coupling. Typically, array elements are placed apart to minimize mutual coupling. However, in MTM arrays, coupling is not only desired but also enhanced and adjusted to increase array bandwidth.

(ii) Much Smaller Array Elements. The coupled array concept is concurrently used for miniaturization. The highest frequency operation occurs when the feed-to-feed element separation becomes $\lambda_o/2$ since multiple lobes will appear beyond this frequency. As an example, to achieve 10 : 1 bandwidth, the feed-to-feed distance between dipole elements must be $\lambda_o/20$ or less at the lowest operating frequency. That is, the interleaving or overlapping of dipoles is not only essential to cancelling the ground plane's inductance but is also critical to achieving large bandwidths.
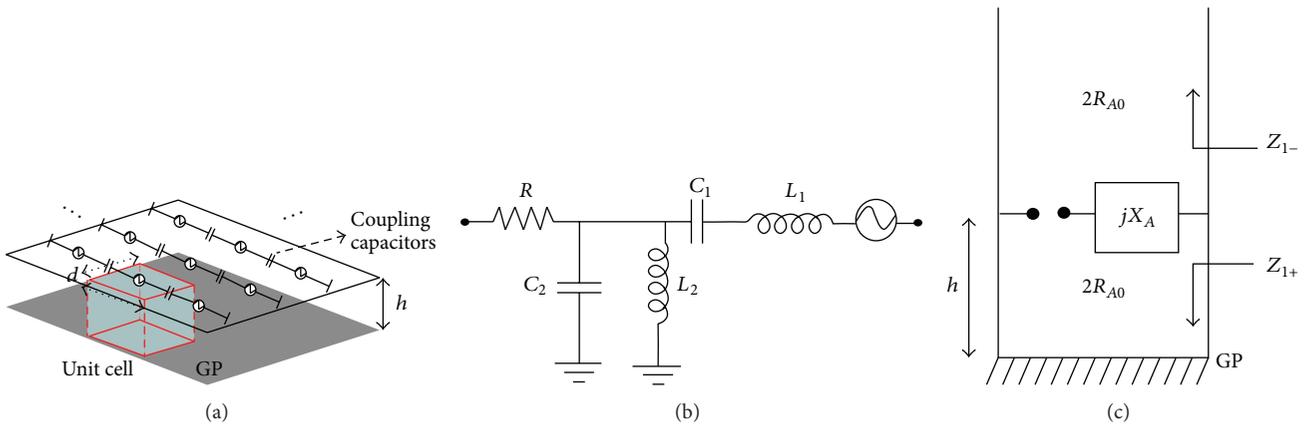
FIGURE 3: (a) General representation of the metamaterial (MTM) array with definition of unit cell, (b) equivalent circuit of MTM array unit cell, and (c) transmission line circuit representation of the array on a ground plane from [46].
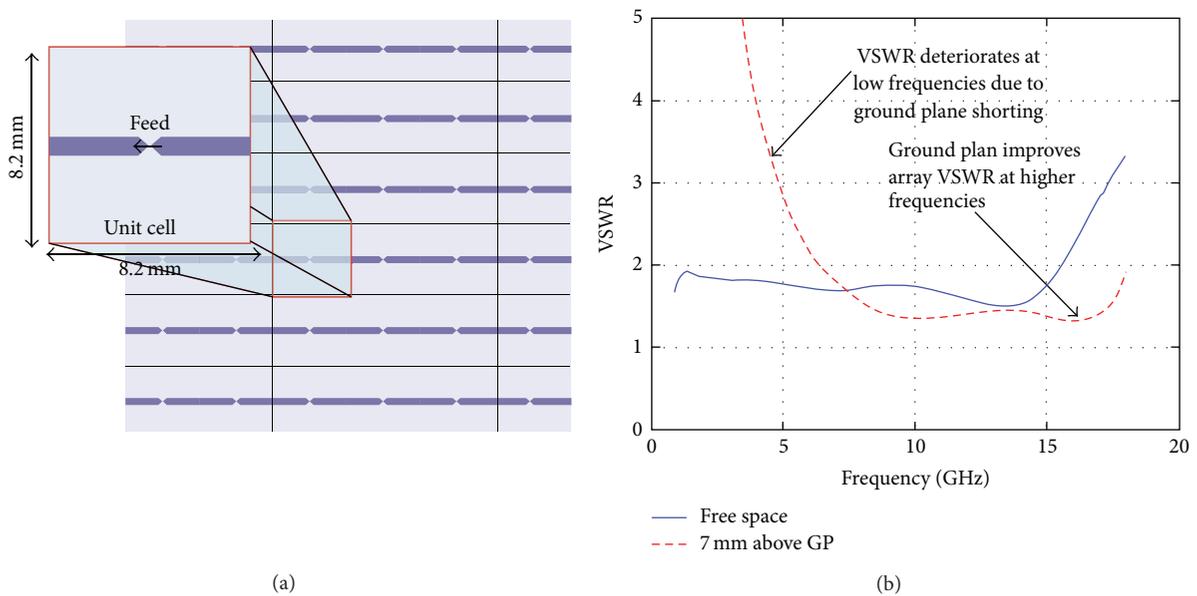

FIGURE 4: VSWR for a tightly coupled dipole array (TCDA) when radiating in free space or in presence of a metallic ground plane from [46].

(iii) Ground Plane (GP) Impedance. In standard arrays, the GP is used as a reflecting surface with often undesirable results. However, in MTM arrays the GP impedance (which is inductive) becomes part of the design and is tuned to increase array bandwidth. As depicted in Figures 4 and 5, a simplistic interconnected dipole array exhibits much better performance at higher frequencies (and over wide bandwidth) when placed above a ground plane. The ground plane height typically becomes $h = \lambda_o/7$ at the highest operational frequency and as small as $h = \lambda_o/70$ at the lowest operational frequency to achieve a 10 : 1 bandwidth.

(iv) Balanced Feeds across the Entire Bandwidth. The printed Marchand-type balun shown in Figure 5 is essential to suppressing the common mode whose presence would generate traveling waves within the substrate. Such waves would destructively interfere with the MTM's array radiation,

particularly when the array is scanning towards lower angles. The printed balun is therefore essential for good scanning performance and for impedance matching, namely, for transitioning the coax feed's 50 Ω impedance to the array's port impedance across the entire bandwidth. Typically, TCDA array's impedance is around 180 Ω. For the feed approach used in Figure 5, a single Wilkinson divider is used to feed a pair of dipoles with their Marchand baluns. Thus, the unit cell becomes a pair of dipoles and not the typical single dipole. This is done to double the impedance of the balun itself for improved matching at the dipole terminals. The details of this concept are depicted in Figure 6 [50].

(v) Superstrate. The superstrate of the TCDA array (see Figure 5) plays an important role. It improves the MTM array bandwidth by reducing the effective size of the array elements and reduces the array impedance to facilitate matching with
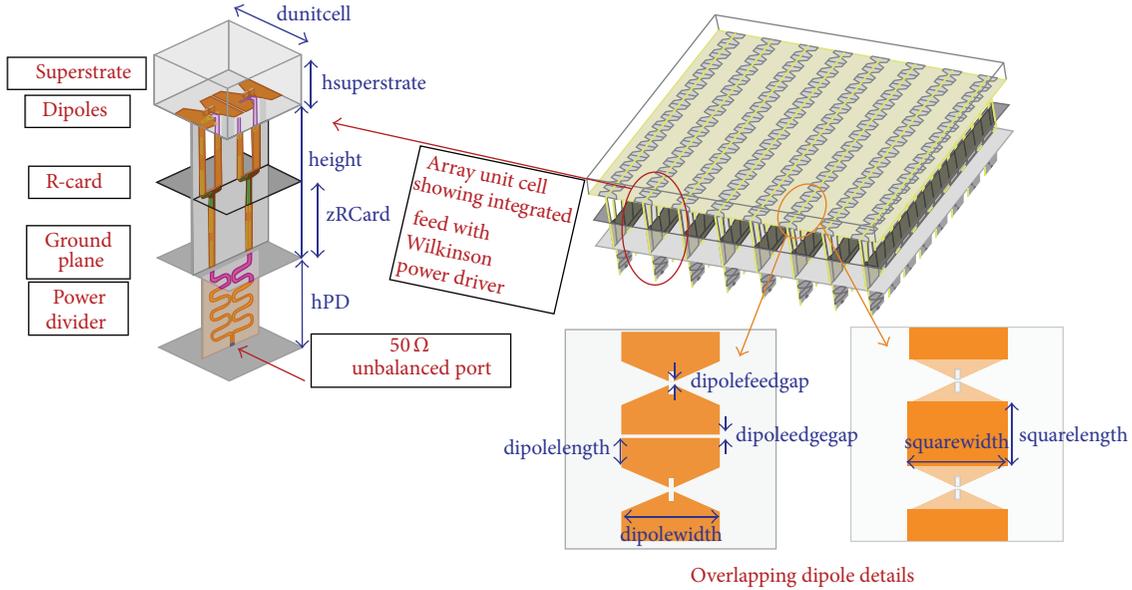
FIGURE 5: Illustration of the tightly coupled dipole array (TCDA) integrated with a balun to create the TCDA-IB array. Enhanced coupling between dipole is achieved using overlapping dipoles at the array's surface. The Marchand-type balun is depicted to the left and a single feed is used to feed a pair of dipoles (creating the unit cell) to double the impedance from the Wilkinson divider for improved matching at the dipole terminals.

the lower feed impedance. It further improves scanning, a concept that has been well exploited in arrays and creates a lensing effect to reduce substrate fields that may cause undesirable surface effects. As is usually the case, its permittivity cannot be too large so as not to negatively affect the array's VSWR and bandwidth.

In the next section, we proceed to discuss a specific TCDA-IB array, providing information on its geometry and measured performance. This array is designed to operate from 280 MHz to 2800 MHz using a ground plane that is only $\lambda_o/10$ in thickness at 2800 GHz and $\lambda_o/100$ thick at the lowest operational frequency. Subsequently, the balun of this class of arrays is reconfigured using switches and LC loads to realize smaller operational bandwidths or even band rejections.

3. Design and Performance of a 10 : 1 MTM Array

The successful TCDA-IB arrays in [50, 51] provided a methodology for designing conformal ultra wideband MTM arrays. In this section, we follow this procedure to design a lower frequency TCDA-IB array with 10 : 1 bandwidth operating across 280 MHz to 2800 MHz. This class of arrays will be used in the next section for reconfiguration. To improve the bandwidth and scanning, parameters of the TCDA-IB array, we pursued a reoptimization of its various parameters. The size of this redesigned array was 10.36 cm (as compared to 6.22 cm in [51]) to achieve greater than 0 dB gain from 280 MHz to 2800 MHz. Also, the array aperture size was increased to 54.33 cm × 54.33 cm. The details are depicted in Figures 7 and 8. After reoptimization of all geometrical

TABLE 1: Values of the all parameters used for the construction of the TCDA-IB array depicted in Figures 5–9.

Model parameter	Value	Model parameter	Value
dunitcell	56.6 mm	dipolelength	7.8 mm
height	103.1 mm	diplewidth	26.7 mm
hsuperstrate	33.3 mm	squarelength	16.7 mm
zRCard	51.6 mm	squarewidth	26.7 mm
hPD	60 mm	dipoleedgegap	1.2 mm
extralength	3.3 mm	subthickness	24 mil
dgnd	4.1 mm	dipolesubthickness	12 mil
dshort	8.3 mm	dipolegap	1.2 mm
zshort	45.9 mm	subedge	10 mil
zopen	21.3 mm	ddipolecon	2.5 mm
dopen	2.0 mm	zdipolecon	2.2 mm
dtrace1	7 mil	dtransition	3.1 mm
dtrace2	11 mil	subthickness	24 mil
dtrace3	13.2 mil	dipolesubthickness	12 mil
rvias	8.3 mil	dipolegap	1.2 mm
dvias	13.3 mil		

parameters, we obtained the dimensions listed in Figure 8 and Table 1.

The overall TCDA-IB structure was constructed using a total of sixteen printed circuit boards (PCBs) placed vertically below the aperture as depicted in Figure 5. Out of these PCBs, 8 constituted the feed baluns (see Figure 7). The other 8 were associated with the printed dipoles. As illustrated in Figure 10, the whole structure is then enclosed in a frame with a Styrofoam molding (if needed) to support the
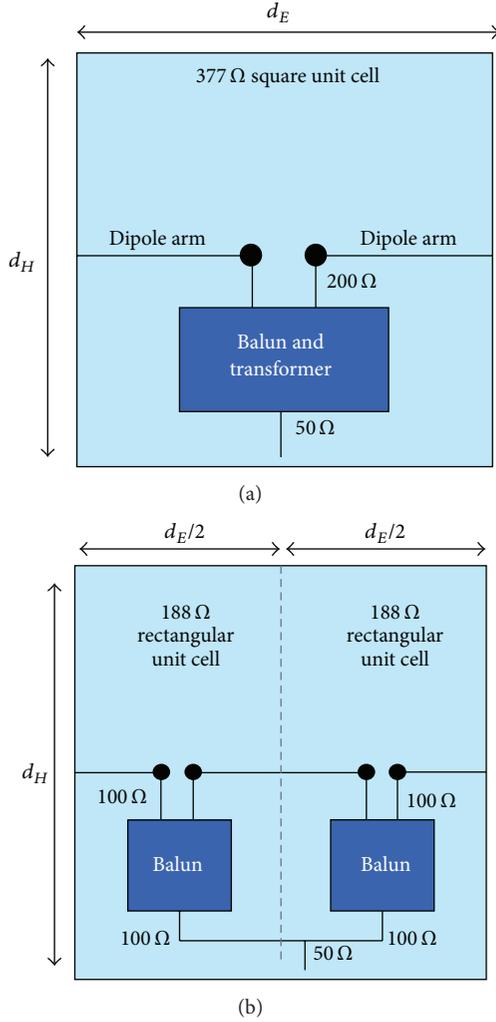
(a)

(b)

FIGURE 6: Impedance of array unit cell is proportional to the aspect ratio of d_E/d_H. Splitting the cell vertically into two halves, the impedance is reduced by a factor of two. Combining the halves in parallel reduces the impedance by another factor of two (power divider from 50 Ω to 100 Ω). (a) Square 377 Ω unit cell and (b) two 188 Ω "half" unit cells from [48].
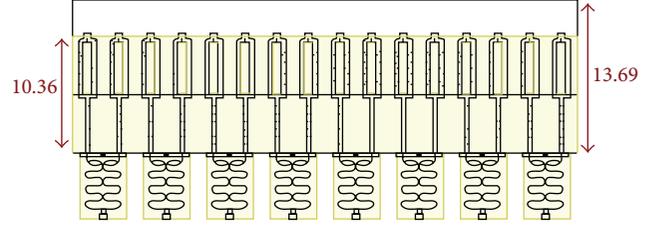

FIGURE 7: Detail of the 8 PCB boards balun feeds with the Winkinson divider below the ground plane. All dimensions are in cm.
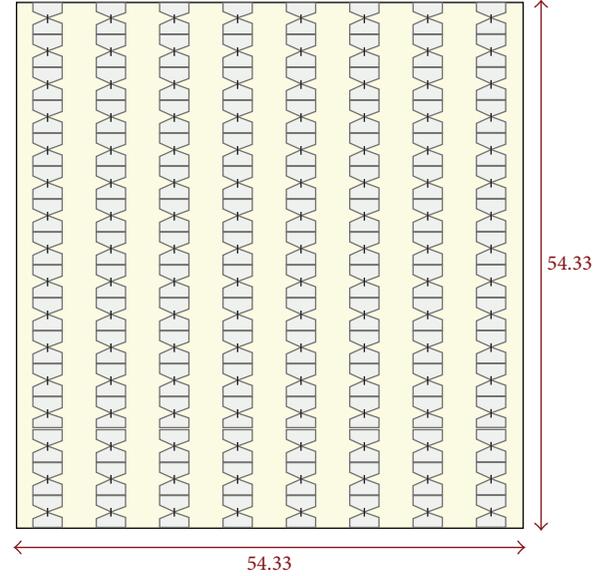

FIGURE 8: Dipole arrangement of the TCDA-IB array in Figure 6 forming the top of the 8 × 8 unit cell array (16 × 16 bowtie dipoles). All dimensions are in cm.

aperture. Photos at different stages of the assembly process for constructing the TCDA-IB are provided in Figure 10. As shown in these photos, the PCBs for the feeds are placed vertically with respect to the array plane. These feeding boards are then held in place by a set of metal rods placed just under the ground plane. The gaps between the feeding boards are then filled with Styrofoam to make the structure stable and easy to handle. It is important to note that the Styrofoam does not impact the array's performance as its permittivity is comparable to air. The dipole PCBs are placed on top and parallel to the ground plane. It is important to note that the dipole PCB boards include strategically placed slots within the bowtie dipoles for anchoring the balun feed ends (see parameter *ddipolecon* in Figure 9). A low loss polyethylene superstrate 3.33 cm thick and having a relative dielectric constant of $\varepsilon_r = 2:25$, with a loss tangent of $\tan \delta = 0.0007$

was placed on top of the array PCB [68] for improving efficiency and scanning. If needed, a resistive sheet can be placed between the dipole array and the ground plane to improve bandwidth at the expense of aperture efficiency. For the case discussed in [49], the aperture efficiency is greater than 70%. It should be noted that the efficiency with the R-card included is no worse than 70% and reaches its lowest value when the ground plane thickness is around $\lambda/2$.

Measurements were conducted by exciting each array port separately while the other 63 ports were terminated in 50 Ω. The UEAEP method [69] was then used to synthesize the gain and patterns at different scan angles. The cross pol was also calculated using Ludwig's 3rd definition [70]. We remark that 2 identical versions of the TCDA-IB array were constructed and measured. These are referred to as Antenna 1 and Antenna 2 in the gain data given in Figure 11. As demonstrated, the measured 8 × 8 array measurements are in complete agreement with calculations, delivering >0 dB realized gain across a 10 : 1 bandwidth. It is important to note that the VSWR bandwidth can be defined to show greater bandwidths. For our design, the simulated VSWR is depicted in Figure 12 showing a VSWR < 2.5 from 200 MHz to about
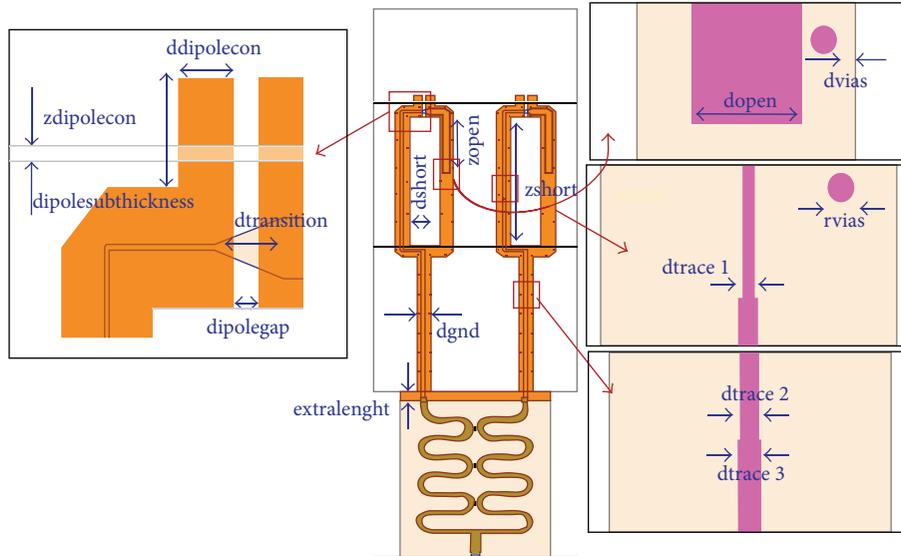
FIGURE 9: Parameter definitions for the TCDA-IB array are shown in Figure 5. This figure provides a listing of the various geometrical parameters that define the integrated balun. Values for the shown parameters are given in Table 1.

FIGURE 10: Fabrication stages of the TCDA-IB array depicted in Figures 5–9. The lower right figure refers to the measurement setup in the Ohio State's compact range. The feeding antenna during measurements is a linearly polarized horn as the array itself is also linearly polarized. Note that the array was measured in the presence of a metallic ground plane of 360 cm × 240 cm in size.

FIGURE 11: Measured and simulated realized gain at broadside (co-pol/E-pol data) for the TCDA-IB array whose geometry is presented in Figures 5–10. The agreement among all 3 g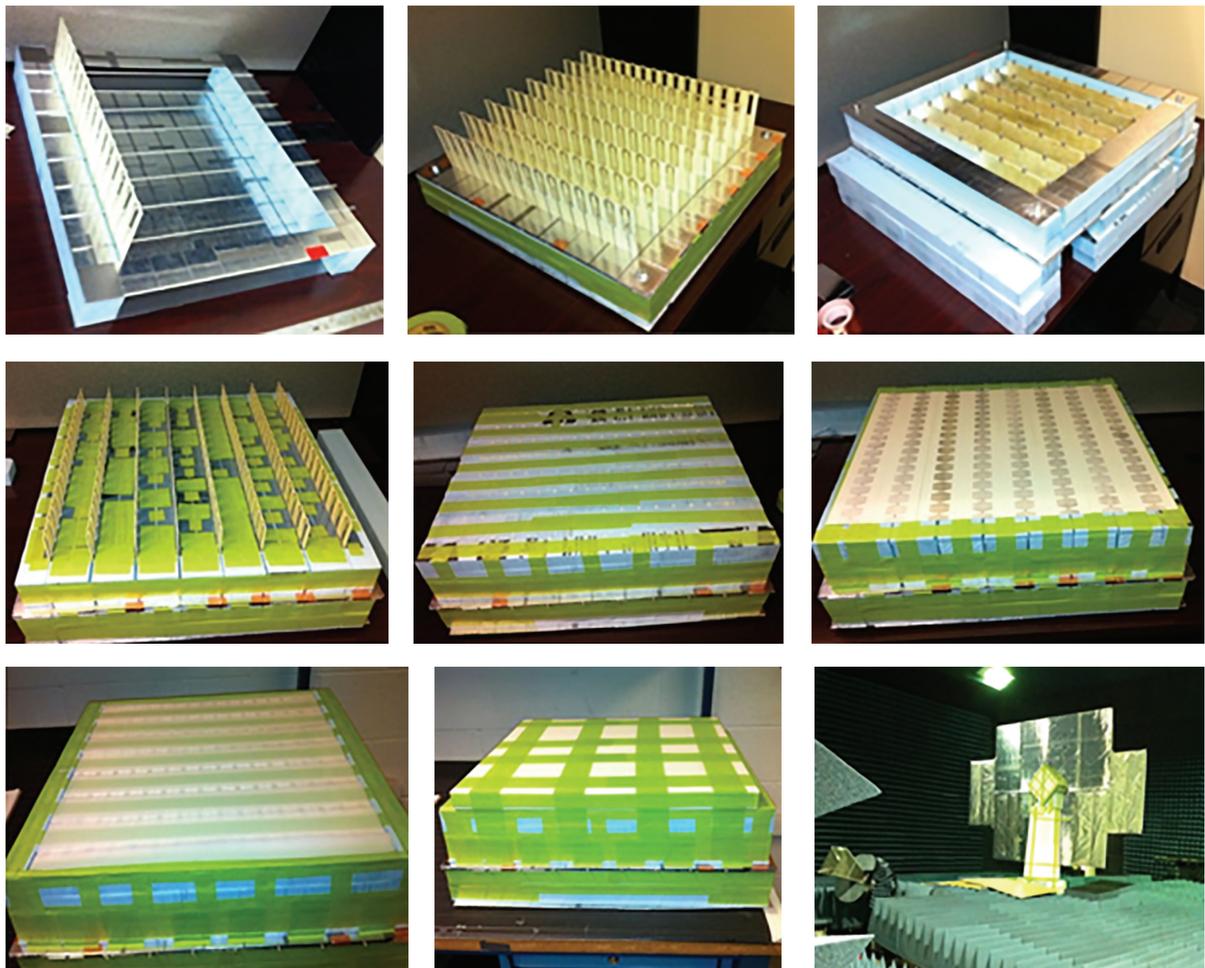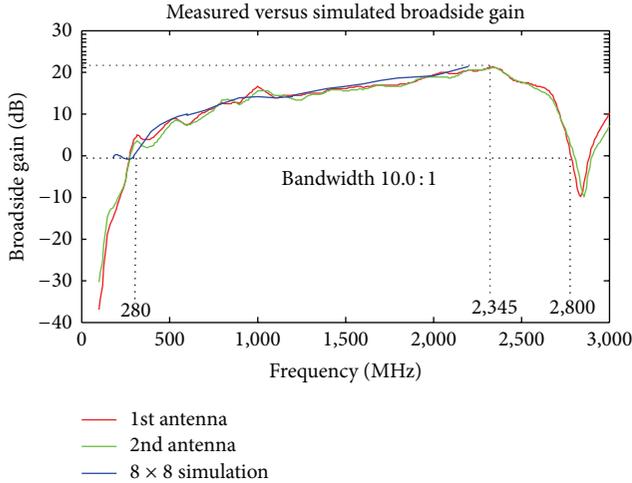ain curves provides substantial confidence in the validity of the measured performance. Small fluctuations in the realized gain are attributed to the horn used for calibration during measurements.
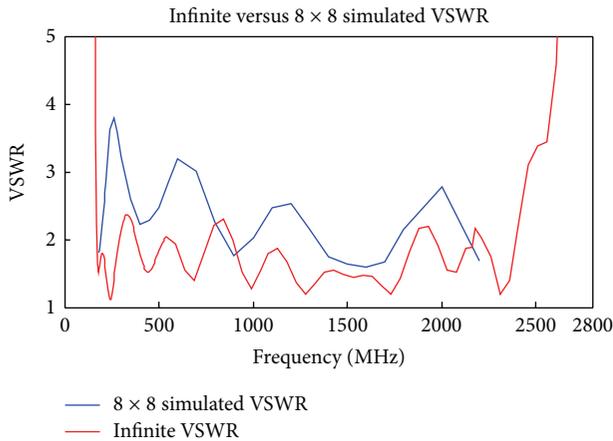

FIGURE 12: VSWR comparison of the infinite versus 8×8 finite TCDA-IB array defined in Figures 5–9. It is noted that the truncation effects of the edge elements of the 8×8 array are responsible for the higher VSWR associated with the 8×8 array.

2400 MHz. This implied a 12 : 1 bandwidth for the infinite array. Because of the array's optimization, this bandwidth is a bit greater than that given in [51] which reaches a bandwidth of 9.2 : 1 with a VSWR < 3. Of course, the finite 8×8 array will have a larger VSWR due to truncation effects of the periphery elements. Indeed, simulations of the 8×8 array shown in Figure 12 demonstrate the larger VSWR.

The beam scanning performance of the fabricated TCDA-IB array in Figure 10 was measured at 600 MHz, 1200 MHz, 1800 MHz, and 2400 MHz. Figures 13 and 14 show the scanned patterns at 0, ±15, ±30, and ±45 degrees for these frequencies. Specifically, Figure 13 shows the E-plane (polarization parallel to the dipoles) patterns and Figure 14 refers

to the H-plane patterns. It is indeed impressive to observe the nearly perfect agreement between the measured and simulated scan patterns. Moreover, the cross-polarization levels are 20–30 dB below the copolarization curves.

It is well known that the worst cross-polarization occurs while scanning in the diagonal plane (D-plane). Therefore, our measurements in this plane were carefully completed. Specifically, time gating was used during measurements to remove diffractions from the ground plane edges. The measured patterns are depicted in Figure 15. As in the case of the co-pol measurements, we again observe distinct lobes while scanning. Moreover, the cross-polarization levels remain 20 dB below the copolarized gain level.

Having validated this TCDA-IB array design, we next proceed to introduce methods for reconfiguring the bandwidth of this class of arrays. Specifically, we introduce methods to reduce its bandwidth or to simply reject a defined set of frequencies across its wide operating bandwidth.

4. Bandwidth Reconfigurable Metamaterial Array

Bandwidth reconfiguration of the MTM array in Figures 2 and 5 can be accomplished in one of three locations outlined in Figure 16. Specifically, we can choose to (1) reconfigure the geometry of the dipoles across the aperture using switches to control the interelement capacitance, (2) integrate filters or geometrically reconfigure the Marchand balun feed depicted more simplistically in Figure 2, and (3) reconfigure the ground plane's location, impedance or by introducing a frequency selective surface (FSS) in place of the resistive sheet depicted in Figure 5. Indeed, the possibilities for array bandwidth/impedance reconfiguration are rather extensive and have yet to be exploited for this class of arrays. We may actually view the EBG ground planes [64] and FSS insertions [63] as reconfigurations that belong to the 3rd category noted above and in Figure 16. However, in the authors' opinion, reconfiguration of the aperture or the ground planes can be challenging to accomplish in practice and may not offer as much flexibility. Specifically, switches within the aperture are difficult integrate with the superstrate. In the case of ground plane reconfigurations, the number of parameters to control is limited and cumbersome to implement. By contrast, reconfiguration of the Marchand balun offers several control parameters. Among them are the balun's stripline impedance, short circuit, and open circuit stublengths and impedances. Below, we consider these options in more detail and provide reconfiguration examples.

To better assess the reconfiguration options, it is important to first cast the array aperture and its feeding configuration into an equivalent circuit. The steps to doing so are depicted in Figure 17. Indeed, the transmission line representation at the top of Figure 17 is precise as it provides circuit parameters to account for the aperture (dipole elements), superstrate, substrate, ground plane, and balun. We note that the balanced feed can be characterized by the microstrip line impedance, Z_1, the open stub's impedance, Z_{OC}, and the short stub's impedance, Z_{SC}. The corresponding geometrical

(a) Radiation pattern of the TCDA-IB array at ±45, ±30, ±15, and 0 deg from broadside at 2.4 GHz

(b) Radiation pattern of the TCDA-IB array at ±45, ±30, ±15, and 0 deg from broadside at 1.8 GHz

(c) Radiation pattern of the TCDA-IB array at ±45, ±30, ±15, and 0 deg from broadside at 1.2 GHz

(d) Radiation pattern of the TCDA-IB array at ±45, ±30, ±15, and 0 deg from broadside at 0.6 GHz
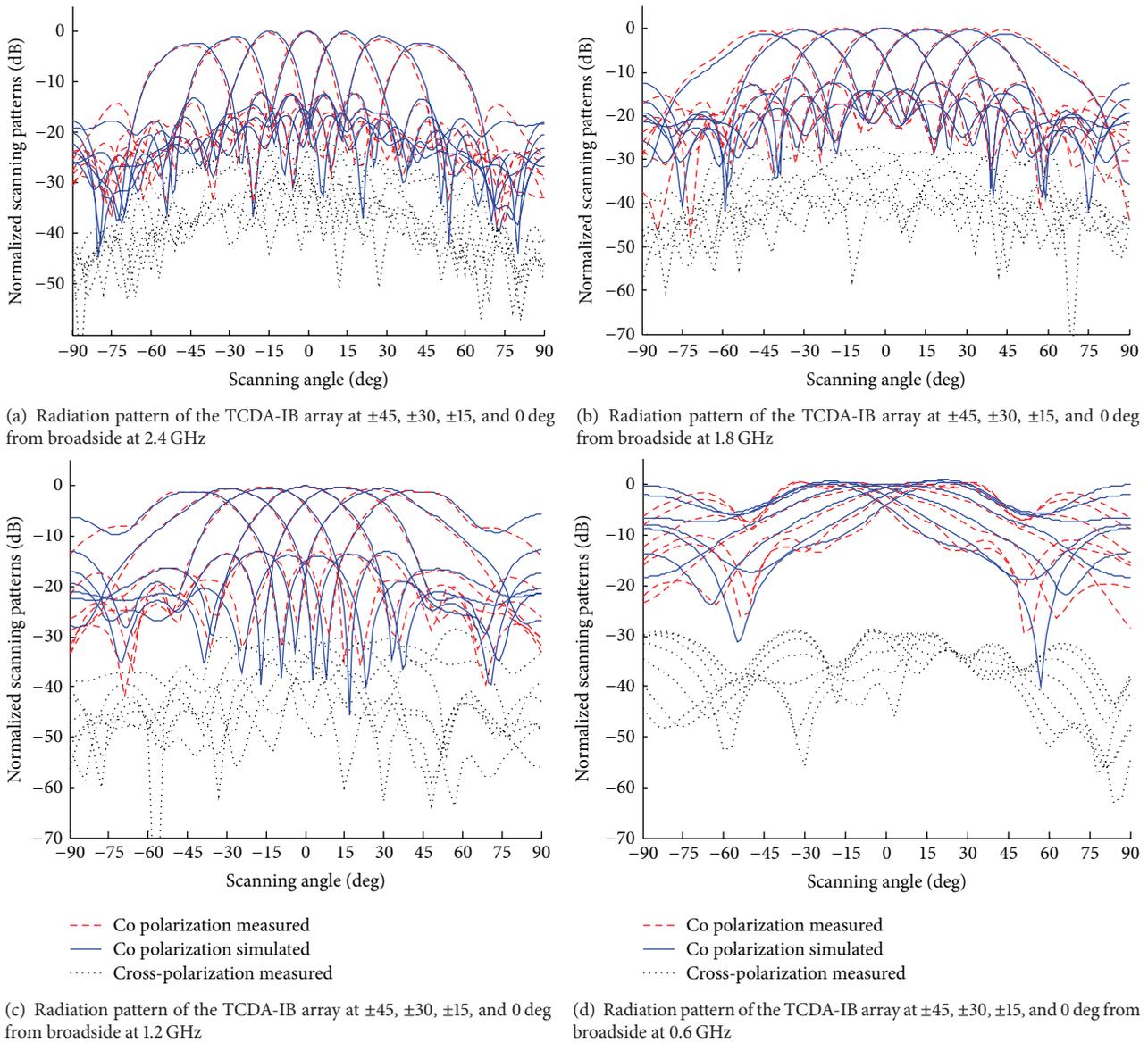
FIGURE 13: E-plane scanning for the TCDA-IB array defined in Figures 5–9. Comparison of measured versus simulated patterns at various scan angles. The measured cross-polarization levels are also included.

components are noted by the circled numbers 2, 3, and 4 at the top of Figure 17. We assert that modification and control of these parameters allow for substantial and full control of the MTM array's band-pass and band-rejection features. However, in modifying the parameters Z_{OC} and Z_{SC}, it is important to concurrently keep in mind the fundamental operation of the balun as depicted in Figure 18. Specifically, the short circuit stub (closed loop in the geometry) ensures that the common mode is suppressed using a symmetric geometry. Therefore, modification of Z_{SC} can only be realized by making the loop or the stub shorter. However, both sides of the loop need to be kept identical to ensure cancellation of the common mode. On the other hand, Z_{OC} can be modified in a more arbitrary fashion. The possibilities are rather broad, and below we demonstrate that modification/control of Z_{OC} allows for substantial control.

As a first step in modifying Z_{OC} we consider the simplified equivalent circuit in Figure 19 implemented on a substrate using microstrip line traces as depicted in Figures 2 and 5. The goal in designing this wideband balun is to ensure that Z_{in} is maintained close to the feedline's characteristic impedance Z_1. For the Marchand balun, it is necessary that Z_{OC} and Z_{SC} satisfy the condition $Z_{OC} \ll Z_{bal} \ll Z_{SC}$, where Z_{bal} is the impedance at the antenna terminals and must be ideally kept equal to the complex conjugate of Z_{TCDA} across the band of interest. In reconfiguring the MTM array's performance our goal is to ensure that Z_{bal} matches Z_{TCDA} only for the band of interest or is highly mismatched across the band rejection of interest.

To demonstrate MTM bandwidth reconfiguration, we proceed to use the equivalent circuit in Figure 19 and optimize its parameters within Agilent's Advanced Design System

(a) Radiation pattern of the TCDA-IB array at ±45, ±30, ±15, and 0 deg from broadside at 2.4 GHz

(b) Radiation pattern of the TCDA-IB array at ±45, ±30, ±15, and 0 deg from broadside at 1.8 GHz

--- Co polarization measured
—— Co polarization simulated
······ Cross-polarization measured

(c) Radiation pattern of the TCDA-IB array at ±45, ±30, ±15, and 0 deg from broadside at 1.2 GHz

--- Co polarization measured
—— Co polarization simulated
······ Cross-polarization measured

(d) Radiation pattern of the TCDA-IB array at ±45, ±30, ±15, and 0 deg from broadside at 0.6 GHz
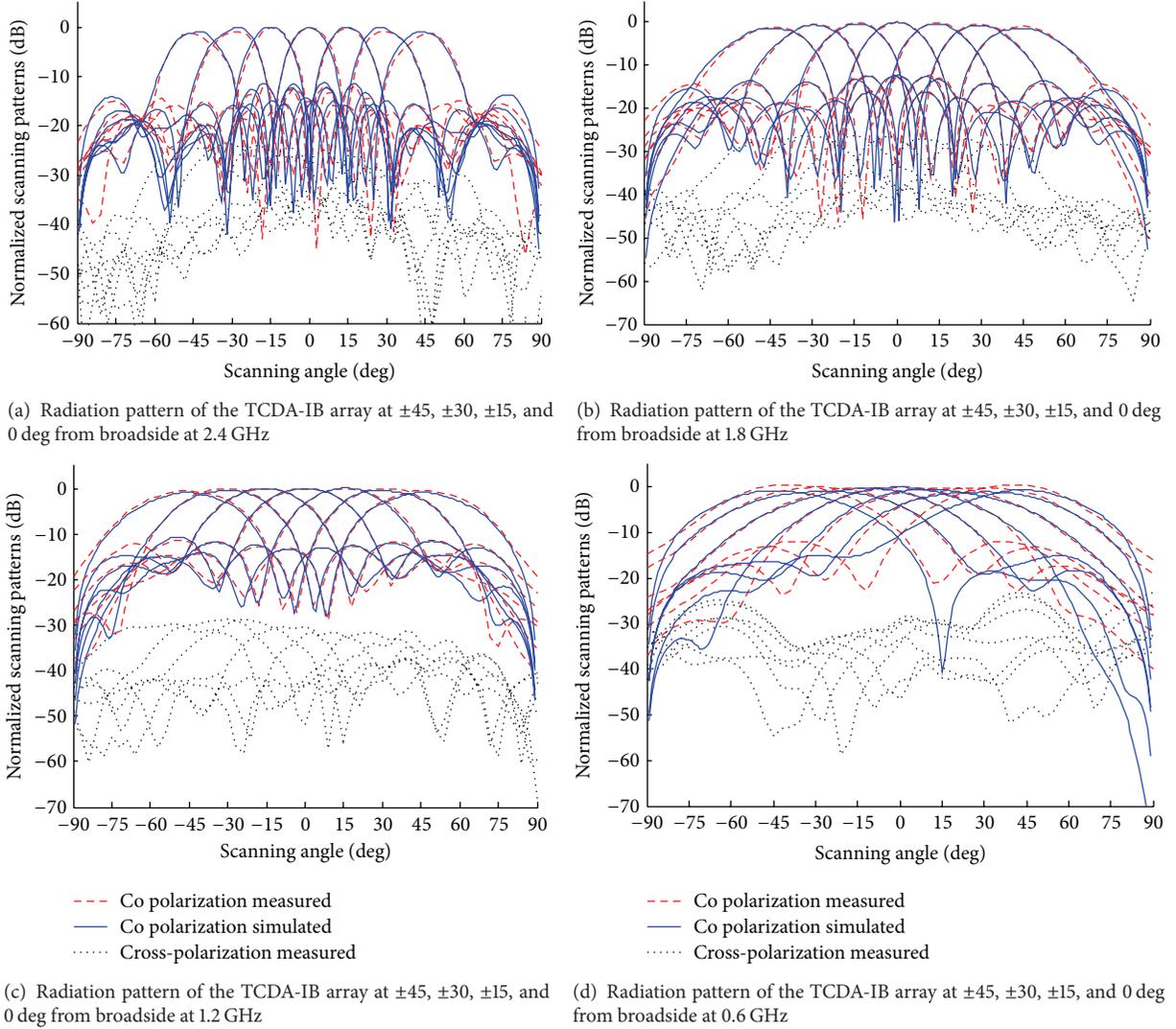
FIGURE 14: H-plane scanning for the TCDA-IB array defined in Figures 5–9. Comparison of the measured versus simulated patterns at various scan angles. The measured cross-polarization levels are also included.

(ADS). As a first step, we select the parameters as follows: $Z_{Feed} = 100\,\Omega$, $Z_0 = Z_{Sub} = Z_{Sup} = 188.5\,\Omega$, $L_{dipole} = 2.2\,pF$, $C_{coupling} = 2.3\,pF$, $h_{sup} = 60°$, $h_{sub} = 90°$, characteristic impedance of $Z_{SC} = 312\,\Omega$, $l_{SC} = 58°$ all defined at 2.5 GHz. Also, we chose $Z_1 = 78\,\Omega$ and $l_1 = 66°$. Using these parameters, we next proceeded to only modify Z_{OC} and observe the bandwidth of the MTM array for various choices. Specifically, as depicted in Figure 20, a load is inserted at the end of the open stub consisting of a series inductor (L_1) and capacitor (C_1) and a shunt (from the stub to the ground) inserted inductor (L_2) and capacitor (C_2). For greater flexibility, a switch SW1 can be closed or open to effectively short out the L_1 and C_1 loads.

Table 2 provides 5 different reconfiguration states of the L_1, C_1, L_2, and C_2 and SW1 parameter choices. The chosen states include the cases as follows.

State 1: $L_2 = 2.5\,nH$ is the only load turned on using SW1 and a switch that activates the load.

State 2: $C_2 = 1.75\,pF$ is the only load turned on using SW1 and a switch that activates the load.

State 3: $L_2 = 2.5\,nH$ and $C_2 = 1.75\,pF$, both turned on (but not L_1 and C_1).

State 4: only $L_1 = 1.3\,nH$ and $C_1 = 3\,pF$ are activated.

State 5: completely absent load at the termination of the open stub (unconfigured).

The last state (State 5) is simply the broadband MTM array as originally designed and shown in Figure 20. The VSWR responses for the other 4 states are depicted in Figure 21. We observe that States 1 and 2 correspond to narrow band-pass bandwidths at the edges of the original unconfigured VSWR response of the MTM array. State 3 refers to another band-pass response in the middle of the MTM's array original unconfigured bandwidth. Finally, State 4 shows a band-rejection response realized with $L_1 = 1.3\,nH$ and $C_1 = 3\,pF$ at the terminals of the open stub in the balun.

(a) Radiation pattern of the TCDA-IB array at ±45, ±30, ±15, and 0 deg from broadside at 2.4 GHz

(b) Radiation pattern of the TCDA-IB array at ±45, ±30, ±15, and 0 deg from broadside at 1.8 GHz

(c) Radiation pattern of the TCDA-IB array at ±45, ±30, ±15, and 0 deg from broadside at 2.4 GHz

(d) Radiation pattern of the TCDA-IB array at ±45, ±30, ±15, and 0 deg from broadside at 1.8 GHz
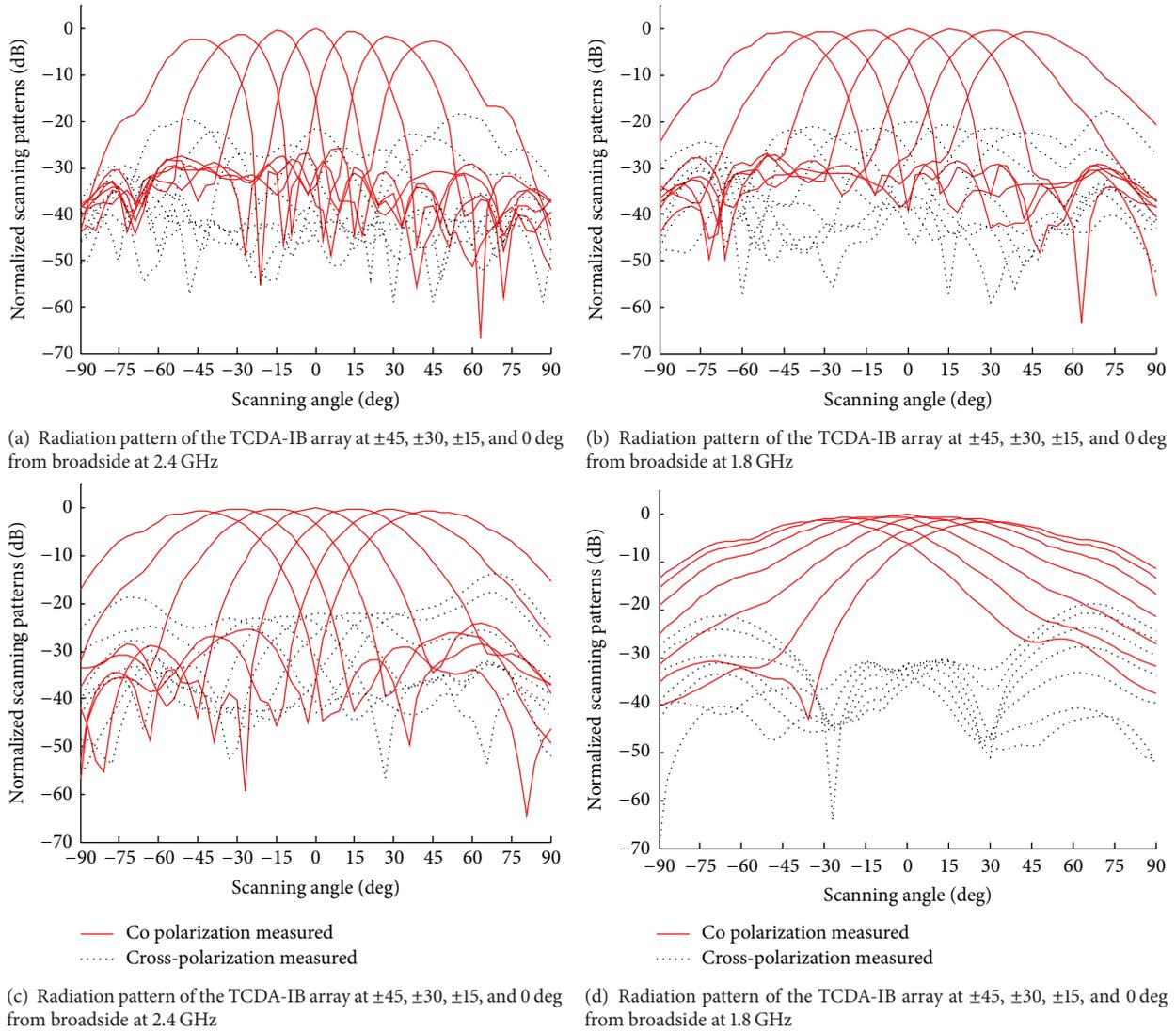
FIGURE 15: Measured diagonal plane scanning for the TCDA-IB array defined in Figures 5–9. No simulation data is available due to demanding computational complexity as symmetry cannot be applied to ease the computational burden. The cross-polarization levels are also included.
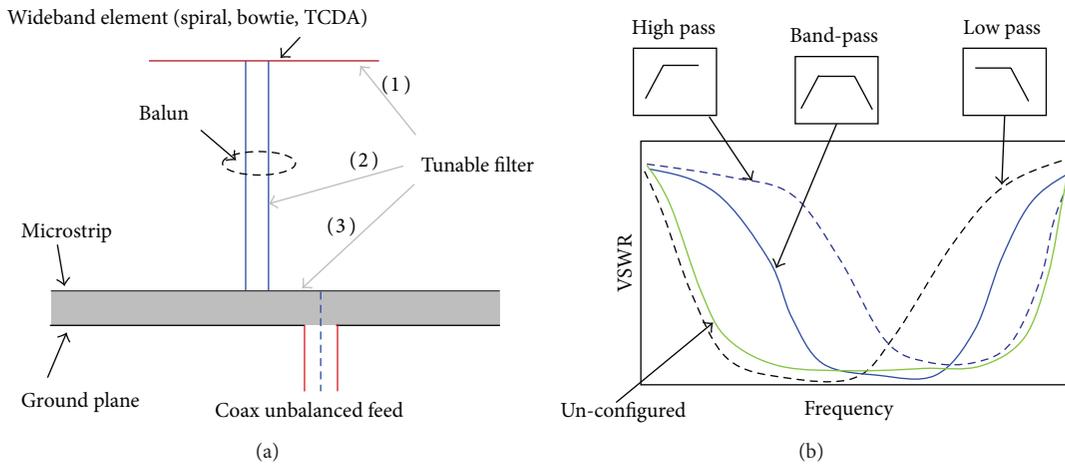

FIGURE 16: Bandwidth reconfiguration concepts: (a) tunable filtering integrated in the aperture (1), feed (balun) (2), or the ground plane (3); (b) representative bandwidth response due to reconfiguration.
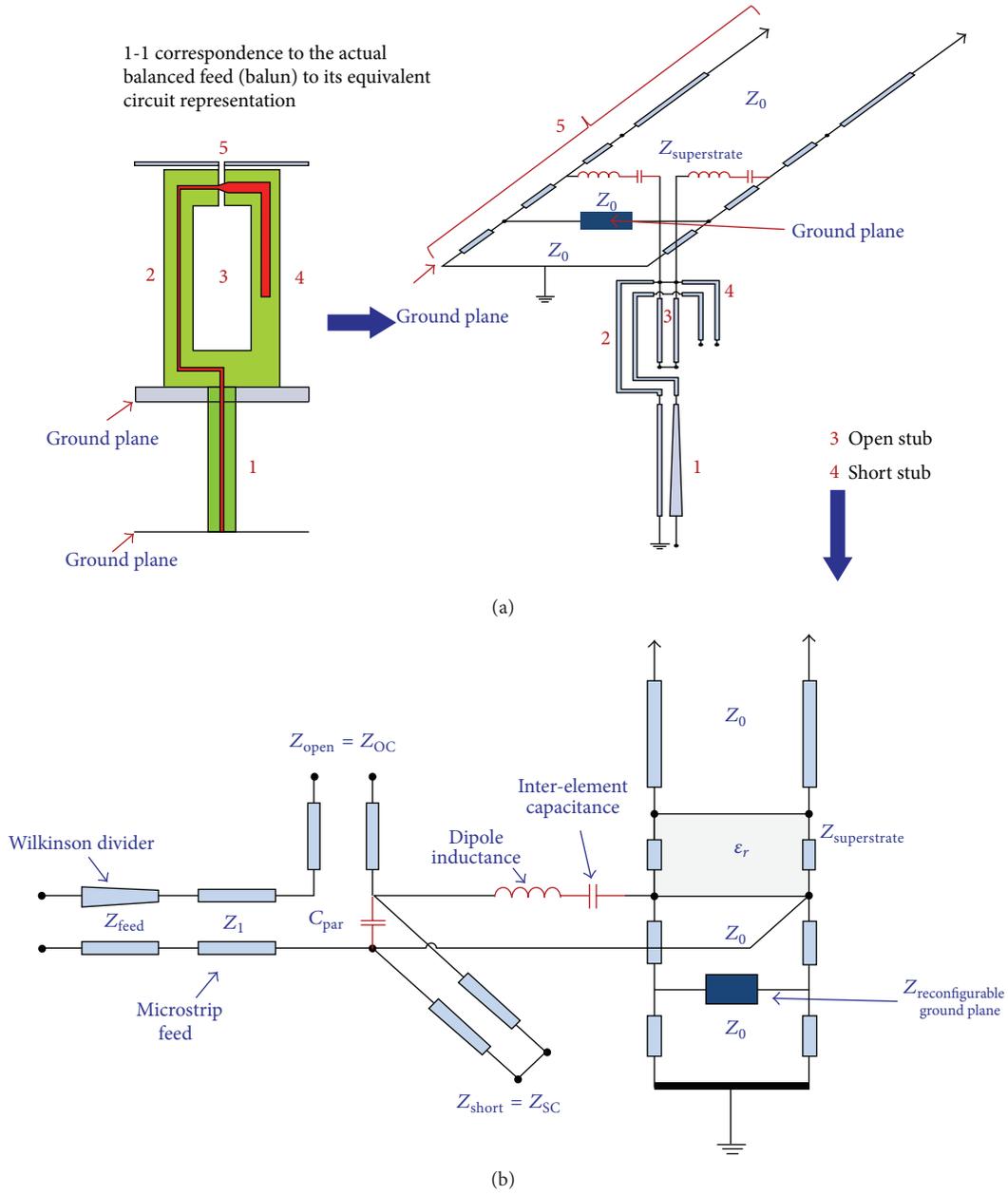
(a)

(b)

FIGURE 17: Equivalent circuit representation of the TCDA-IB array in Figure 5. The top graphic provides a one to one correspondence between the Marchand balun in Figure 2 and its equivalent transmission line circuit representation. The bottom circuit is a recasting of the equivalent transmission line circuit into a more typical RF circuit showing the open (Z_{OC}) and short circuit (Z_{SC}) impedances of the balun itself.

TABLE 2: MTM array performance for various choices of the load termination of the open stub.

Chosen state	SW1	C_1	L_1	C_2	L_2	Configuration	Bandwidth (%)	Bandwidth (MHz)
1	X				X	high Pass	9.3	400
2	X			X		low Pass	58	515
3	X			X	X	bandpass	53	1,300
4		X	X			band-stop	22*	565*
5		unconfigured				UWB	161	3,960

X = activated (on)/closed switch; no marker = deactivated (off)/open switch.
Bandwidth is listed for VSWR < 3; *indicates band rejection bandwidth.
$C_1 = 3$ pF, $L_1 = 1.3$ nH, $C_2 = 1.75$ pF, and $L_2 = 2.5$ nH.
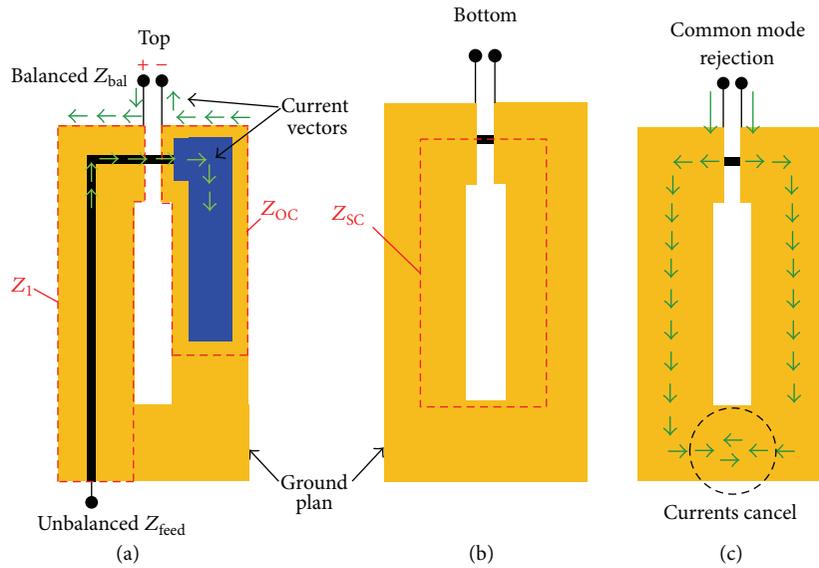All other MTM array circuit parameters are given in Figure 20.

FIGURE 18: MTM array microstrip balun functionality depicting balanced currents and common mode rejection.
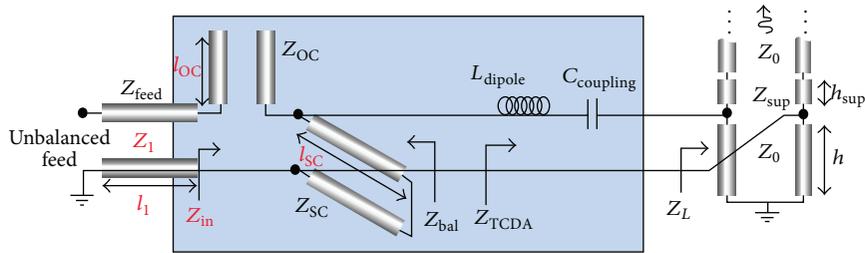

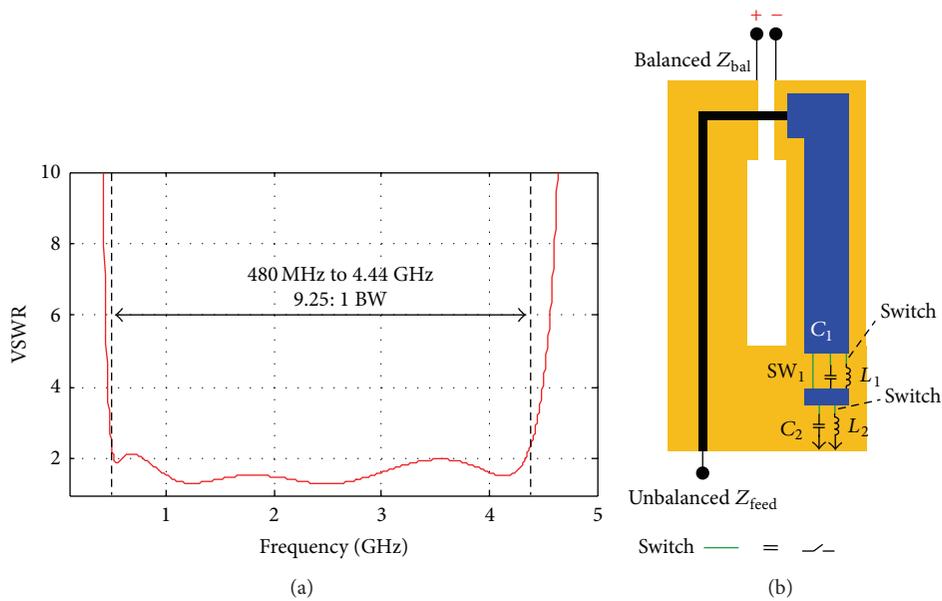FIGURE 19: Simplified Marchand balun equivalent circuit (see [48]).

FIGURE 20: MTM array bandwidth reconfiguration by varying the loads at the termination of the open stub. For the VSWR response to the left stub it is simply left open, implying SW1 is open and C_2/L_2 are off (unconfigured case). The other parameters: $Z_{\text{Feed}} = 100\,\Omega$, $Z_0 = Z_{\text{Sub}} = Z_{\text{Sup}} = 188.5\,\Omega$, $L_{\text{dipole}} = 2.2\,\text{nH}$, $C_{\text{coupling}} = 2.3\,\text{pF}$, $h_{\text{sup}} = 60°$, $h_{\text{sub}} = 90°$, characteristic impedance of $Z_{\text{OC}} = 11\,\Omega$, $l_{\text{oc}} = 87°$, characteristic impedance of $Z_{\text{SC}} = 312\,\Omega$, $l_{\text{SC}} = 58°$ with all electrical lengths given at 2.5 GHz.
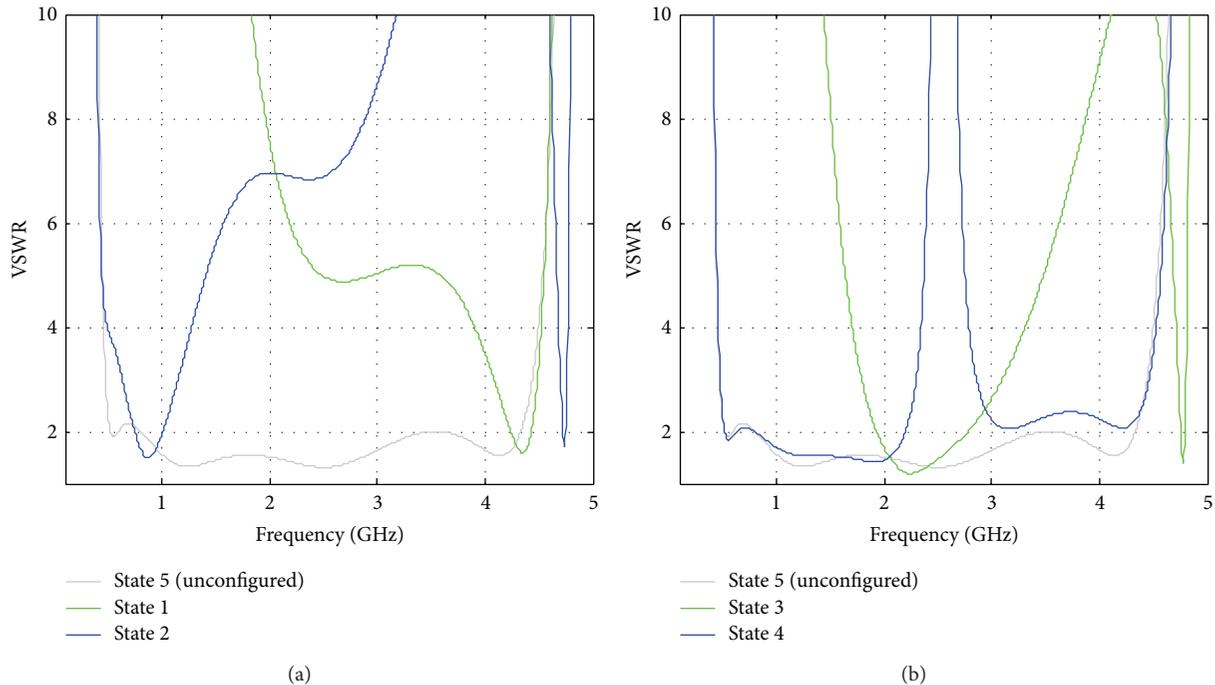
(a)

(b)

Figure 21: VSWR versus frequency for Table 2 reconfiguration states.

The above reconfiguration choices indicate that we have significant control in generating band-pass and band-rejection responses starting with the broadband MTM array in Figures 2 and 5. Moreover, bandwidth reconfiguration is achieved using simple loads at the terminal of the open stub of the balun feed behind the MTM array. We can achieve any response across the original MTM array bandwidth by simply using varactors to change C_1 and C_2 and/or MEMS switches as reported in [71] or pin diodes to change the length of the open or shorted stubs in the balun. Also, the load's reactive impedance can be realized in practice using variable length stubs. Both, the MEMS switches and capacitor banks are known to have low losses. Therefore, their impact on the overall antenna performance should be quite small. If varactors are necessary for continuous precise tuning, care in choosing the optimum low-loss component would be imperative. Maximum allowable loss would dictate the highest tuning ratio attainable by the varactor diode.

5. Concluding Remarks

In this paper we reviewed the concept of conformal wideband metamaterial (MTM) arrays with as much as 10 : 1 continuous bandwidth in the presence of realistic feeds. MTM array design guidelines and performance validation were provided via measurements. Array scanning was demonstrated and we noted that a key aspect of the broadband response was due to (a) the array's interelement coupling to cancel the inductance stemming from the ground plane and (b) the balun feed that suppressed common modes and achieved impedance matching across the entire bandwidth.

Equivalent circuit representations of the array were presented to aid in the design and reconfiguration of the array. These circuit representations were used to develop simple bandwidth reconfiguration schemes. Instead of reconfiguring the geometry of the antenna's aperture or the ground plane, we instead resorted to simple changes in the microstrip lines present in the balanced feed. It was shown that the addition of simple lumped capacitors or inductors at the stub's termination can provide substantial bandwidth control by simply switching on or off the load inductors or capacitors.

Conflict of Interests

The authors declare that there is no conflict of interests regarding the publication of this paper.

References

[1] G. V. Eleftheriades and N. Engheta, "Metamaterials: fundamentals and applications in the microwave and optical regimes," *Proceedings of the IEEE*, vol. 99, no. 10, pp. 1618–1621, 2011.

[2] N. Engheta and R. W. Ziolkowski, *Electromagnetic Metamaterials: Physics and Engineering Explorations*, John Wiley & Sons, Hoboken, NJ, USA, 2006.

[3] G. V. Eleftheriades and K. G. Balmain, *Negative Refraction Metamaterials: Fundamental Principles and Applications*, John Wiley & Sons-IEEE Press, Hoboken, NJ, USA, 2005.

[4] D. H. Werner and D. H. Kwon, *Transformation Electromagnetics and Metamaterials: Fundamental Principles and Applications*, Springer, London, UK, 2014.

[5] F. Capolino, *Theory and Phenomena of Metamaterials*, vol. 1-2, CRC Press, Taylor & Francis Group, Boca Raton, Fla, USA, 2009.

[6] C. Caloz and T. Itoh, *Electromagnetic Metamaterials: Transmission Line Theory and Microwave Applications*, Wiley-IEEE Press, 2005.

[7] J. L. Volakis, C. C. Chen, and K. Fujimoto, *Small Antennas: Miniaturization Techniques and Applications*, McGraw Hill, New York, NY, USA, 2010.

[8] M. C. Scardelletti, G. E. Ponchak, S. Merritt, J. S. Minor, and C. A. Zorman, "Electrically small folded slot antenna utilizing capacitive loaded slot lines," in *Proceedings of the IEEE Radio and Wireless Symposium (RWS '08)*, pp. 731–734, January 2008.

[9] J.-H. Lu and K.-L. Wong, "Slot-loaded, meandered rectangular microstrip antenna with compact dual-frequency operation," *Electronics Letters*, vol. 34, no. 11, pp. 1048–1050, 1998.

[10] A. Holub and M. Polívka, "A novel microstrip patch antenna miniaturization technique: meanderly folded shorted-patch antenna," in *Proceedings of the 14th Conference on Microwave Techniques (COMITE '08)*, pp. 1–4, April 2008.

[11] M. Lee, B. A. Kramer, C.-C. Chen, and J. L. Volakis, "Distributed lumped loads and lossy transmission line model for wideband spiral antenna miniaturization and characterization," *IEEE Transactions on Antennas and Propagation*, vol. 55, no. 10, pp. 2671–2678, 2007.

[12] R. W. Ziolkowski and A. Erentok, "Metamaterial-based efficient electrically small antennas," *IEEE Transactions on Antennas and Propagation*, vol. 54, no. 7, pp. 2113–2130, 2006.

[13] F. Qureshi, M. A. Antoniades, and G. V. Eleftheriades, "A compact and low-profile metamaterial ring antenna with vertical polarization," *IEEE Antennas and Wireless Propagation Letters*, vol. 4, no. 1, pp. 333–336, 2005.

[14] M. A. Antoniades and G. V. Eleftheriades, "A folded-monopole model for electrically small NRI-TL metamaterial antennas," *IEEE Antennas and Wireless Propagation Letters*, vol. 7, pp. 425–428, 2008.

[15] K. M. K. H. Leong, C.-J. Lee, and T. Itoh, "Compact metamaterial based antennas for MIMO applications," in *Proceedings of the IEEE International Workshop on Antenna Technology: Small and Smart Antennas Metamaterials and Applications (iWAT '07)*, pp. 87–90, March 2007.

[16] G. Mumcu, K. Sertel, and J. L. Volakis, "Miniature antennas and arrays embedded within magnetic photonic crystals," *IEEE Antennas and Wireless Propagation Letters*, vol. 5, no. 1, pp. 168–171, 2006.

[17] G. Mumcu, K. Sertel, J. L. Volakis, I. Vitebskiy, and A. Figotin, "RF propagation in finite thickness unidirectional magnetic photonic crystals," *IEEE Transactions on Antennas and Propagation*, vol. 53, no. 12, pp. 4026–4034, 2005.

[18] S. Yarga, K. Sertel, and J. L. Volakis, "Degenerate band edge crystals for directive antennas," *IEEE Transactions on Antennas and Propagation*, vol. 56, no. 1, pp. 119–126, 2008.

[19] S. Lim, C. Caloz, and T. Itoh, "Metamaterial-based electronically controlled transmission-line structure as a novel leaky-wave antenna with tunable radiation angle and beamwidth," *IEEE Transactions on Microwave Theory and Techniques*, vol. 53, no. 1, pp. 161–172, 2005.

[20] A. Rennings, T. Liebig, S. Otto, C. Caloz, and I. Wolff, "Highly directive resonator antennas based on composite right/left-handed (CRLH) transmission lines," in *Proceedings of the 2nd International ITG Conference on Antennas (INICA '07)*, pp. 190–194, March 2007.

[21] N. Apaydin, K. Sertel, and J. L. Volakis, "Nonreciprocal leaky-wave antenna based on coupled microstrip lines on a non-uniformly biased ferrite substrate," *IEEE Transactions on Antennas and Propagation*, vol. 61, no. 7, pp. 3458–3465, 2013.

[22] D. Sievenpiper, J. Schaffner, J. J. Lee, and S. Livingston, "A steerable leaky-wave antenna using a tunable impedance ground plane," *IEEE Antennas and Wireless Propagation Letters*, vol. 1, pp. 179–182, 2002.

[23] Z. H. Jiang, Q. Wu, and D. H. Werner, "Demonstration of enhanced broadband unidirectional electromagnetic radiation enabled by a subwavelength profile leaky anisotropic zero-index metamaterial coating," *Physical Review B. Condensed Matter and Materials Physics*, vol. 86, no. 12, Article ID 125131, 2012.

[24] C. G. Christodoulou, Y. Tawk, S. A. Lane, and S. R. Erwin, "Reconfigurable antennas for wireless and space applications," *Proceedings of the IEEE*, vol. 100, no. 7, pp. 2250–2261, 2012.

[25] J. T. Bernhard, "Reconfigurable antennas," in *Antenna Engineering Handbook*, J. Volakis, Ed., McGraw Hill, New York, NY, USA, 2007.

[26] J. K. Smith, "Reconfigurable aperture antenna (RECAP)," DARP, 1999, http://www.darpa.mil.

[27] E. R. Brown, "RF-MEMS switches for reconfigurable integrated circuits," *IEEE Transactions on Microwave Theory and Techniques*, vol. 46, no. 11, pp. 1868–1880, 1998.

[28] G. H. Huff and J. T. Bernhard, "Integration of packaged RF MEMS switches with radiation pattern reconfigurable square spiral microstrip antennas," *IEEE Transactions on Antennas and Propagation*, vol. 54, no. 2, pp. 464–469, 2006.

[29] G. Rebeiz, *RF MEMS: Theory, Design, and Technology*, John Wiley & Sons, 2004.

[30] W. M. Zhu, H. Cai, T. Mei et al., "A MEMS tunable metamaterial filter," in *Proceedings of the 23rd IEEE International Conference on Micro Electro Mechanical Systems (MEMS '10)*, pp. 196–199, January 2010.

[31] A. Grau, J. Romeu, M.-J. Lee, S. Blanch, L. Jofre, and F. De Flaviis, "A Dual-Linearly-polarized MEMS-reconfigurable antenna for narrowband MIMO communication systems," *IEEE Transactions on Antennas and Propagation*, vol. 58, no. 1, pp. 4–17, 2010.

[32] W. Zhang, W. M. Zhu, J. M. Tsai et al., "Thz polarizer using tunable metamaterials," in *Proceedings of the IEEE 26th International Conference on Micro Electro Mechanical Systems (MEMS '13)*, pp. 713–716, January 2013.

[33] D. Peroulis, K. Sarabandi, and L. P. B. Katehi, "Design of reconfigurable slot antennas," *IEEE Transactions on Antennas and Propagation*, vol. 53, no. 2, pp. 645–654, 2005.

[34] S. Shelley, J. Costantine, C. G. Christodoulou, D. E. Anagnostou, and J. C. Lyke, "FPGA-controlled switch-reconfigured antenna," *IEEE Antennas and Wireless Propagation Letters*, vol. 9, pp. 355–358, 2010.

[35] C. R. White and G. M. Rebeiz, "Single- and dual-polarized tunable slot-ring antennas," *IEEE Transactions on Antennas and Propagation*, vol. 57, no. 1, pp. 19–26, 2009.

[36] H. Jiang, M. Patterson, C. Zhang, and G. Subramanyam, "Frequency tunable microstrip patch antenna using ferroelectric thin film varactor," in *Proceedings of the IEEE National Aerospace and Electronics Conference (NAECON '09)*, pp. 248–250, July 2009.

[37] S.-S. Oh, Y.-B. Jung, Y.-R. Ju, and H.-D. Park, "Frequency-tunable open-ring microstrip antenna using varactor," in *Proceedings of the 12th International Conference on Electromagnetics in Advanced Applications (ICEAA '10)*, pp. 624–626, September 2010.

[38] C. J. Panagamuwa, A. Chauraya, and J. C. Vardaxoglou, "Frequency and beam reconfigurable antenna using photoconducting switches," *IEEE Transactions on Antennas and Propagation*, vol. 54, no. 2, pp. 449–454, 2006.

[39] L. N. Pringle, P. H. Harms, S. P. Blalock et al., "A reconfigurable aperture antenna based on switched links between electrically small metallic patches," *IEEE Transactions on Antennas and Propagation*, vol. 52, no. 6, pp. 1434–1445, 2004.

[40] Y. E. Erdemli, R. A. Gilbert, and J. L. Volakis, "A reconfigurable slot aperture design over a broad-band substrate/feed structure," *IEEE Transactions on Antennas and Propagation*, vol. 52, no. 11, pp. 2860–2870, 2004.

[41] A. Q. Liu, W. M. Zhu, and Q. H. Song, "Microfluidic tunable metamaterial for gigahertz filter array," in *Proceedings of the 17th International Conference on Solid-State Sensors, Actuators and Microsystems (Transducers & Eerosensors '13)*, pp. 2481–2484, June 2013.

[42] K. Jaruwongrungsee, W. Withayachumnankul, A. Wisitsoraat, D. Abbott, C. Fumeaux, and A. Tuantranont, "Metamaterial-inspired microfluidic-based sensor for chemical discrimination," in *Proceedings of the 11th IEEE SENSORS Conference*, pp. 1–4, October 2012.

[43] G. Mumcu, A. Dey, and T. Palomo, "Frequency-agile bandpass filters using liquid metal tunable broadside coupled split ring resonators," *IEEE Microwave and Wireless Components Letters*, vol. 23, no. 4, pp. 187–189, 2013.

[44] Z. H. Jiang, L. Lin, J. A. Bossard, and D. H. Werner, "Bifunctional plasmonic metamaterials enabled by subwavelength nano-notches for broadband, polarization-independent enhanced optical transmission and passive beam-steering," *Optics Express*, vol. 21, no. 25, pp. 31492–31505, 2013.

[45] B. A. Munk, *Finite Antenna Arrays and FSS*, John Wiley & Sons, 2000.

[46] J. L. Volakis and K. Sertel, "Narrowband and wideband metamaterial antennas based on degenerate band edge and magnetic photonic crystals," *Proceedings of the IEEE*, vol. 99, no. 10, pp. 1732–1745, 2011.

[47] I. Tzanidis, K. Sertel, and J. L. Volakis, "Interwoven spiral array (ISPA) with a 10:1 bandwidth on a ground plane," *IEEE Antennas and Wireless Propagation Letters*, vol. 10, pp. 115–118, 2011.

[48] J. Kasemodel, C. C. Chen, and J. L. Volakis, "Wideband conformal array with integrated feed and matching network for wide-angle scanning," *IEEE Transactions on Antennas and Propagation*, vol. 61, no. 9, pp. 4528–4537, 2013.

[49] W. F. Moulder, K. Sertel, and J. L. Volakis, "Superstrate-enhanced ultrawideband tightly coupled array with resistive FSS," *IEEE Transactions on Antennas and Propagation*, vol. 60, no. 9, pp. 4166–4172, 2012.

[50] J. P. Doane, K. Sertel, and J. L. Volakis, "A wideband, wide scanning tightly coupled Dipole array with integrated balun (TCDA-IB)," *IEEE Transactions on Antennas and Propagation*, vol. 61, no. 9, pp. 4538–4548, 2013.

[51] W. F. Moulder, K. Sertel, and J. L. Volakis, "Ultrawideband superstrate-enhanced substrate-loaded array with integrated feed," *IEEE Transactions on Antennas and Propagation*, vol. 61, no. 11, pp. 5802–5807, 2013.

[52] D. H. Schaubert, S. Kasturi, A. O. Boryssenko, and W. M. Elsallal, "Vivaldi antenna arrays for wide bandwidth and electronic scanning," in *Proceedings of the 2nd European Conference on Antennas and Propagation (EuCAP '07)*, pp. 1–6, November 2007.

[53] R. W. Kindt and W. R. Pickles, "Ultrawideband all-metal flared-notch array radiator," *IEEE Transactions on Antennas and Propagation*, vol. 58, no. 11, pp. 3568–3575, 2010.

[54] M. W. Elsallal and J. C. Mather, "An ultra-thin, decade (10:1) Bandwidth, modular BAVA array with low cross-polarization," in *Proceedings of the IEEE International Symposium on Antennas and Propagation and USNC/URSI National Radio Science Meeting (APSURSI '11)*, pp. 1980–1983, July 2011.

[55] D. Cavallo, A. Neto, G. Gerini, A. Micco, and V. Galdi, "A 3-to 5-GHz wideband array of connected dipoles with low cross polarization and wide-scan capability," *IEEE Transactions on Antennas and Propagation*, vol. 61, no. 3, pp. 1148–1154, 2013.

[56] S. S. Holland and M. N. Vouvakis, "The planar ultrawideband modular antenna (PUMA) array," *IEEE Transactions on Antennas and Propagation*, vol. 60, no. 1, pp. 130–140, 2012.

[57] J. P. Doane, K. Sertel, and J. L. Volakis, "Bandwidth limits for lossless planar arrays over ground plane," *Electronics Letters*, vol. 48, no. 10, pp. 540–542, 2012.

[58] J. P. Doane, *Wideband low-profile antenna arrays: fundamental limits and practical implementations [Ph.D. dissertation]*, The Ohio State University, Columbus, Ohio, USA, 2013.

[59] J. G. Maloney, B. N. Baker, R. T. Lee, G. N. Kiesel, and J. J. Acree, "Wide scan, integrated printed circuit board, fragmented aperture array antennas," in *Proceedings of the IEEE International Symposium on Antennas and Propagation and USNC/URSI National Radio Science Meeting (APSURSI '11)*, pp. 1965–1968, July 2011.

[60] N. Marchand, "Transmission-line conversion transformers," *Electronics*, vol. 17, no. 12, pp. 142–145, 1944.

[61] D. M. L. Bartholomew, "Optimum design for a broadband microstrip balun," *Electronics Letters*, vol. 13, no. 17, pp. 510–511, 1977.

[62] F. Erkmen, C.-C. Chen, and J. L. Volakis, "Impedance matched ferrite layers as ground plane treatments to improve antenna wide-band performance," *IEEE Transactions on Antennas and Propagation*, vol. 57, no. 1, pp. 263–266, 2009.

[63] Y. E. Erdemli, K. Sertel, R. A. Gilbert, D. E. Wright, and J. L. Volakis, "Frequency-selective surfaces to enhance performance of broad-band reconfigurable arrays," *IEEE Transactions on Antennas and Propagation*, vol. 50, no. 12, pp. 1716–1724, 2002.

[64] F. Yang and Y. Rahmat-Samii, "Reflection phase characterizations of the EBG ground plane for low profile wire antenna applications," *IEEE Transactions on Antennas and Propagation*, vol. 51, no. 10, pp. 2691–2703, 2003.

[65] F. Yang and Y. Rahmat-Samii, *Electromagnetetic Band Gap Structures in Antenna Engineering*, Cambridge University Press, 2009.

[66] B. Munk, R. Taylor, T. Durham et al., "A low-profile broadband phased array antenna," in *Proceedings of the IEEE International Antennas and Propagation Symposium and USNC/CNC/URSI North American Radio Science Meeting*, pp. 448–451, June 2003.

[67] H. A. Wheeler, "Simple relations derived fom a phased-array antenna made of an infinite current sheet," *IEEE Transactions on Antennas and Propagation*, vol. 13, no. 4, pp. 506–514, 1965.

[68] D. G. Bodnar, "Materials and design data," in *Antenna Engineering Handbook*, J. L. Volakis, Ed., McGraw Hill, 4th edition, 2007.

[69] D. F. Kelley and W. L. Stutzman, "Array antenna pattern modeling methods that include mutual coupling effects," *IEEE Transactions on Antennas and Propagation*, vol. 41, no. 12, pp. 1625–1632, 1993.

[70] J. E. Roy and L. Shafai, "Generalization of the Ludwig-3 definition for linear copolarization and cross polarization," *IEEE Transactions on Antennas and Propagation*, vol. 49, no. 6, pp. 1006–1010, 2001.

[71] A. S. Morris, S. P. Natarajan, Q. Gu, and V. Steel, "Impedance tuners for handsets utilizing high-volume RF-MEMS," in *Proceedings of the 42nd European Microwave Conference (EuMC '12)*, pp. 193–196, November 2012.